Facile fabrication of boron-doped titanium carbide for efficient electrocatalytic nitrogen reduction

Tao Leiming [a,*], Pang Kui [a,b], Qin Wen [a], Huang Liming [a,c], Duan Linhai [a], Zhu Guanhua [a], Li Qiuye [b,*], Yu Changlin [a,*]

[a] *Guangdong Provincial Key Laboratory of Petrochemical Equipment Fault Diagnosis, School of Science, Guangdong University of Petrochemical Technology, Maoming, Guangdong, 525000, China.*

[b] *Engineering Research Center for Nanomaterials, Henan University, Henan, 475001, China*

[c] *School of Chemistry and Chemical Engineering, Guangxi University, Nanning, 530004, China*

[*] Corresponding author. E-mail address：leimingtao@foxmail.com (Tao Leiming), qiuyeli@henu.edu.cn (Li Qiuye), yuchanglinjx@163.com(Yu Changlin)

Supporting information

Experimental section

Materials: Titanium Aluminum Carbide powder (Ti_3AlC_2, 200 mesh), Hydrofluoric Acid (HF, 40%), Potassium hydroxide (KOH), H_2O_2 (30 wt%), Salicylic acid ($C_7H_6O_3$), hydrochloric acid (HCl), sodium hypochlorite (NaClO) and Sodium hydroxide (NaOH), Nafion (5 wt%) solution, Nafion 117 membrane (DuPont). Hydrazine hydrate ($N_2H_4 \cdot H_2O$), Ethanol (CH_3CH_2OH), Sodium citrate dihydrate ($Na_3C_6H_5O_7 \cdot 2H_2O$), p-dimethylaminobenzaldehyde (p-$C_9H_{11}NO$), Sodium nitroso ferricyanide dihydrate ($Na_2[Fe(CN)_5NO] \cdot 2H_2O$), All reagents were analytical grade and were used directly without further purification.

Preparation of working electrode: Carbon paper (CP) was cleaned via

brief sonication with ethanol and water for several times. To prepare the working electrode, the catalyst ink was prepared by dispersing 5 mg of Ti_3C_2–B catalyst dispersed into 1 mL ethanol containing 50 μL of 5 wt% Nafion and kept ultrasonic for 1 h. Then 20 μL of the catalyst ink was loaded on the CP (1 cm × 1 cm) and dried at room temperature.

Preparation of $Ti_3C_2T_x$ nanosheets: 1 g Ti_3AlC_2 was gradually added to 20 mL HF, and then magnetically stirred at room temperature for 24 h. Subsequently. The resulting solution was washed with distilled water, centrifuged at 4000 rpm for 10 min, and repeated several times until the supernatant pH approached 7. Finally, Multi-layer MXenes powder is then collected by freeze-drying. $Ti_3C_2T_x$ flakes were dispersed in 1.8 $mol \cdot L^{-1}$ KOH aqueous solution (1 g MXene per 20 mL KOH aqueous solution). Then, the final product was washed using DI water for several times and dried as Ti_3C_2.

Preparation of Ti_3C_2-B nanosheets: 90 mg Ti_3C_2 powder is uniformly dispersed in deionized water. Then, 100 mg H_3BO_3 (the molar ratio of H_3BO_3 to Ti_3C_2 is 3:1) was added to the mixture (3 $mg \cdot mL^{-1}$) and stirred for 0.5 h. The suspension was transferred to a Teflon reactor and heated at 180 ^oC for 12 h to produce a gray-black precipitate. The final product was washed using DI water for several times and dried as Ti_3C_2–B.

Characterizations: X-ray diffraction (XRD) patterns from 5°to 80°were obtained using Cu Ka radiation at a scan rate of 10 $°s^{-1}$ on an UItima IV

X-ray diffractometer with an applied current and accelerating voltage of 40 mA and 40 kV, respectively. SEM images and EDX were characterized on Regulus 8220 scanning electron microscope with an accelerating voltage of 5 kV (HITACHI, Japan). TEM and HR-TEM images were detected by JEOL JEM-2100F (200 kV) transmission electron microscope operated. The XPS was carried out by Thermo Scientific escalab 250Xi. UV-Vis diffuse reflectance (DRS) absorption spectroscopy was performed on a SHIMADZU UV-2600i with $BaSO_4$ as a reference material in a scan range of 200–800 nm. Ion chromatography was used to measure the levels of NH_3 in the electrolytes using a Shine CIC-D100 ion chromatograph. Gas chromatograph (GC-2014C, SHIMADZU).

Electrochemical measurements: N_2 reduction experiments were performed in two compartments of cells under environmental conditions, separated by Nafion 117 membrane. The membrane is protonated by first re-treating in an aqueous H_2O_2 (5 wt %) solution at 80 ^oC for 1 hour. Then, the membrane was immersed in 0.5 M H_2SO_4 at 80 ^oC for 1 hour, and finally immersed in water for 6 hours. Electrochemical measurements were performed using an electrochemical workstation (CHI760E) in a standard three-electrode system, using Ti_2C_3–B / CP (1.0 cm × 1.0 cm) as the working electrode, platinum mesh as the counter electrode and Ag / AgCl electrode (saturated potassium chloride electrolyte) as the reference electrode. All potentials measured are calibrated to reversible hydrogen

electrode (RHE) using the following equation: E (vs. RHE) = E (vs. Ag / AgCl) + 0.059 × pH + 0.197 V, and the current density presented is normalized to the geometric surface area. For N_2 reduction experiments, chronoamperometry was performed at room temperature in N_2-saturated 0.05 M H_2SO_4 solution (N_2 purged H_2SO_4 electrolyte for 60 min before measurement).

Determination of NH_3:

The electro-reduced ammonia was detected by ion chronograph. In specific, 2 mL postelectrolyzed electrolyte was filtered by a nylon membrane filter (220 nm) and then injected directly into the ion chronograph. The NH^{4+} calibration curves were established by a set of standard solutions with different ammonia sulfide concentrations. The signal of NH^{4+} in ion chronograph spectra was located at 4.1 min.

The concentration of NH_3 produced by spectrophotometry was determined by indophenol blue method. Usually, 2 mL of HCl electrolyte is taken out of the cathode chamber and 2 mL of 1 M NaOH solution containing 5 % salicylic acid and 5 % sodium citrate is added to the solution. Subsequently, 1 mL 0.05 M NaClO and 0.2 mL 1 % $C_5FeN_6Na_2O{\cdot}2H_2O$ were added to the above solution in turn. After standing at room temperature for 2 h, the UV-Vis absorption spectra were measured at a wavelength of 655 nm. Concentration-absorbance curves were calibrated with a range of concentrations of NH_3 standard solutions.

The concentration-absorption curve was calibrated in 0.05 M H_2SO_4 using NH_4^+ standard solutions with NH_4^+ concentrations of 0, 0.05,0.1 0.2, 0.4, 0.6, 0.8, and 1.0 μg·mL^{-1}. The calibration curve below is used to calculate the NH_3 concentration. The fitting curve ($y = 0.4862x - 0.00621$, $R^2 = 0.999$) showed a good linear relationship between the absorbance value and the NH_3 concentration through three independent calibrations.

Determination of N_2H_4: The possible presence of N_2H_4 in the electrolyte is estimated by the method of Watt and Chrisp. Usually, p-$C_9H_{11}NO$ (5.99 g), HCl (30 mL) and C_2H_5OH (300 mL) are mixed and used as color reagents. Then, 5 mL of the electrolyte electrochemical reaction container is taken out from the solution, and 5 mL of the prepared color reagent is added. Stir at room temperature for 15 min. In addition, the absorbance of the resulting solution is measured at S6 The wavelength was 455 nm. The concentration absorbance curve was calibrated using a standard N_2H_4 solution with a series of concentrations.

Calculations of NH_3 yield and FE: The FE for N_2 reduction was defined as the amount of electric charge used for synthesizing NH_3 divided the total charge passed through the electrodes during the electrolysis. The total amount of NH_3 produced was measured using colorimetric methods. Assuming three electrons were needed to produce one NH_3 molecule, the FE could be calculated as follows:

$$FE(\%) = \frac{3 \times n_{NH_3} \times F}{Q} \quad (1)$$

Among them, FE (%) is the Faraday efficiency of NH_3, 3 is the electron transfer number of each NH_3 molecule, n_{NH3} is the total amount of ammonia generated during the electrolysis process (in mol), F is the Faraday constant (96485 $C \cdot mol^{-1}$), and Q is the total charge consumed during the electrolysis process (in C).

NH_3 yield was calculated using the following equation:

$$r_{NH_3} = \frac{n_{NH_3}}{t \times m_{cat}} \quad (2)$$

where r_{NH3} is the yield of NH_3, n_{NH3} is the total amount of ammonia produced in the production process, t is the total time of electrolysis, and m_{cat} is the total mass of the catalyst.

DFT Calculations:

In this work, all calculations were carried out with the standard DFT using Vienna ab initio Simulation Package (MedeA-VASP 3.6). The description of the exchange correlation adopted the generalized gradient approximation (GGA) of the Perdew, Burke, and Ernzerhof form. The plane wave energy cutoff was set to 500 eV. The generalized gradient approximation (GGA) with the Perdew-Burke-Ernzerhof (PBE) exchange-correlation functional. The Brillouin zone was sampled at Gamma point with the 2 × 2 × 2 k-point meshes for Ti_3C_2 and Ti_3C_2–B surfaces. The energy and force criterion for convergence of the electron density were set at 10^{-5} eV and 0.5 eV/Å, respectively. The vacuum space along z-direction was set to 19 Å to avoid interactions between adjacent images.

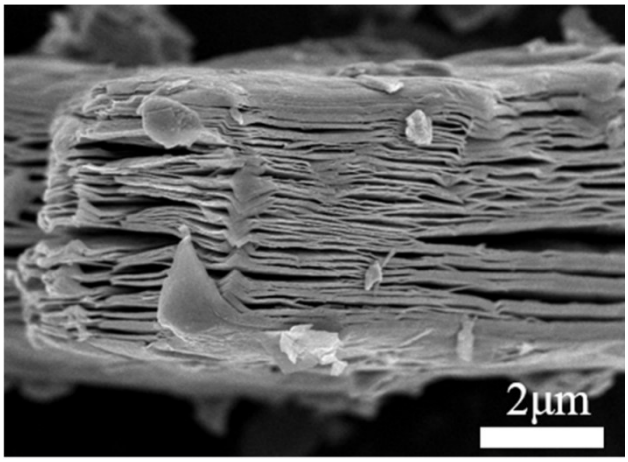

Figure S1. SEM images of Ti_3C_2.

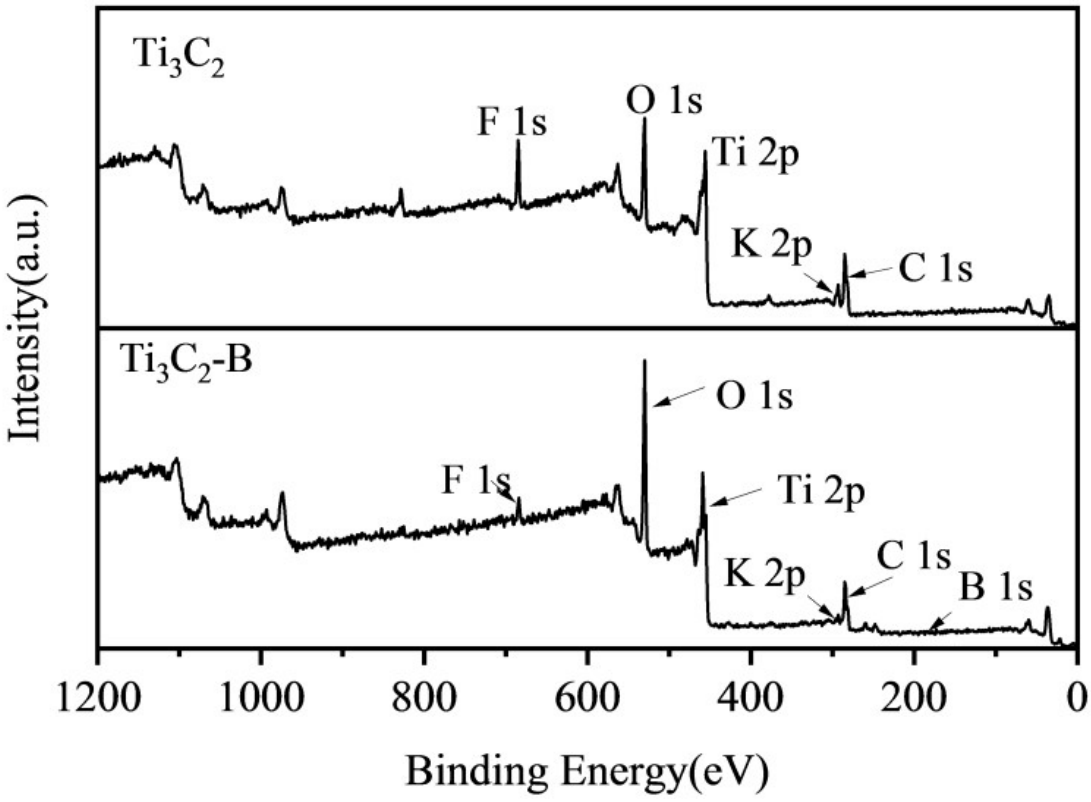

Figure S2. The survey XPS spectra of Ti_3C_2 and Ti_3C_2–B.

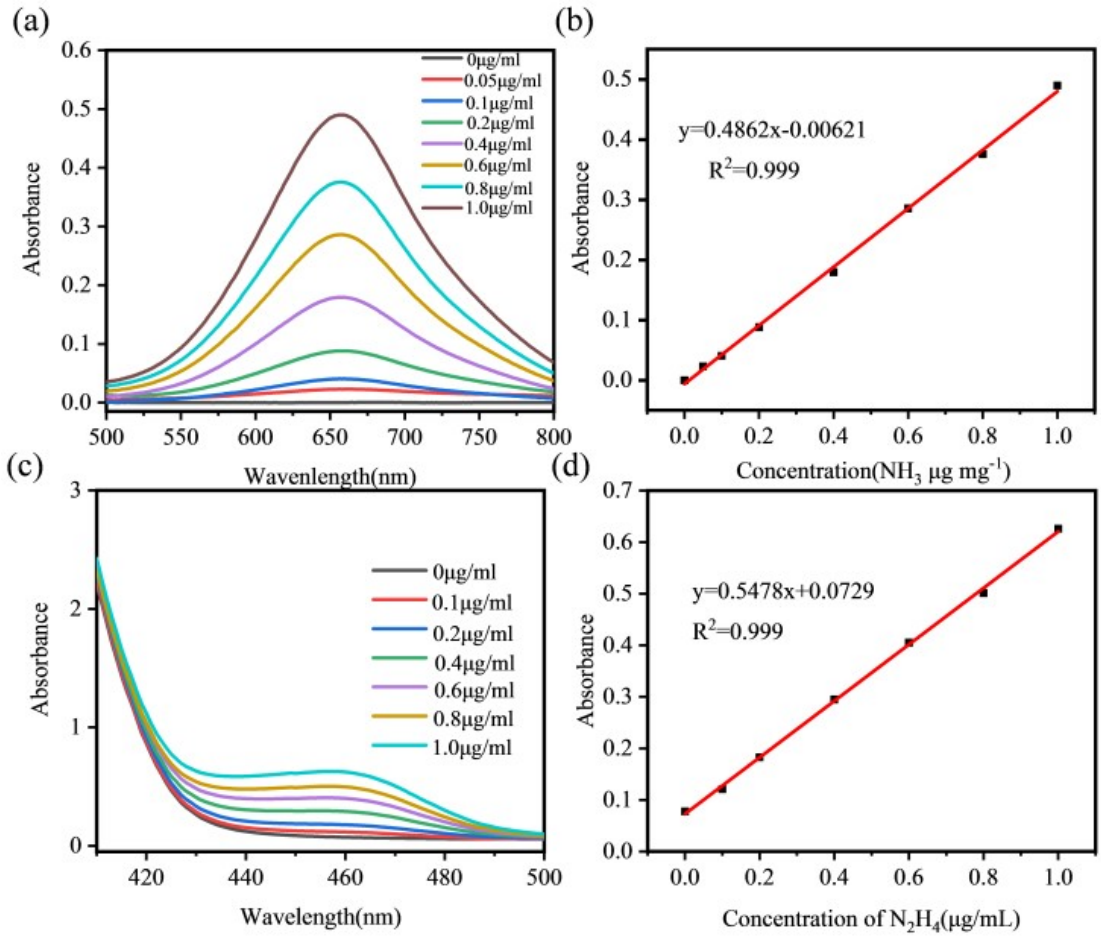

Figure S3. (a) UV-vis absorption spectra of as-prepared references with various NH_3 concentrations after incubated for 2 h. (b) Calibration curve used for calculation of NH_3 concentrations. (c) UV-vis absorption spectra of as-prepared references with various N_2H_4 concentrations after incubated for 15 min. (d) Calibration curve used for calculation of N_2H_4 concentrations.

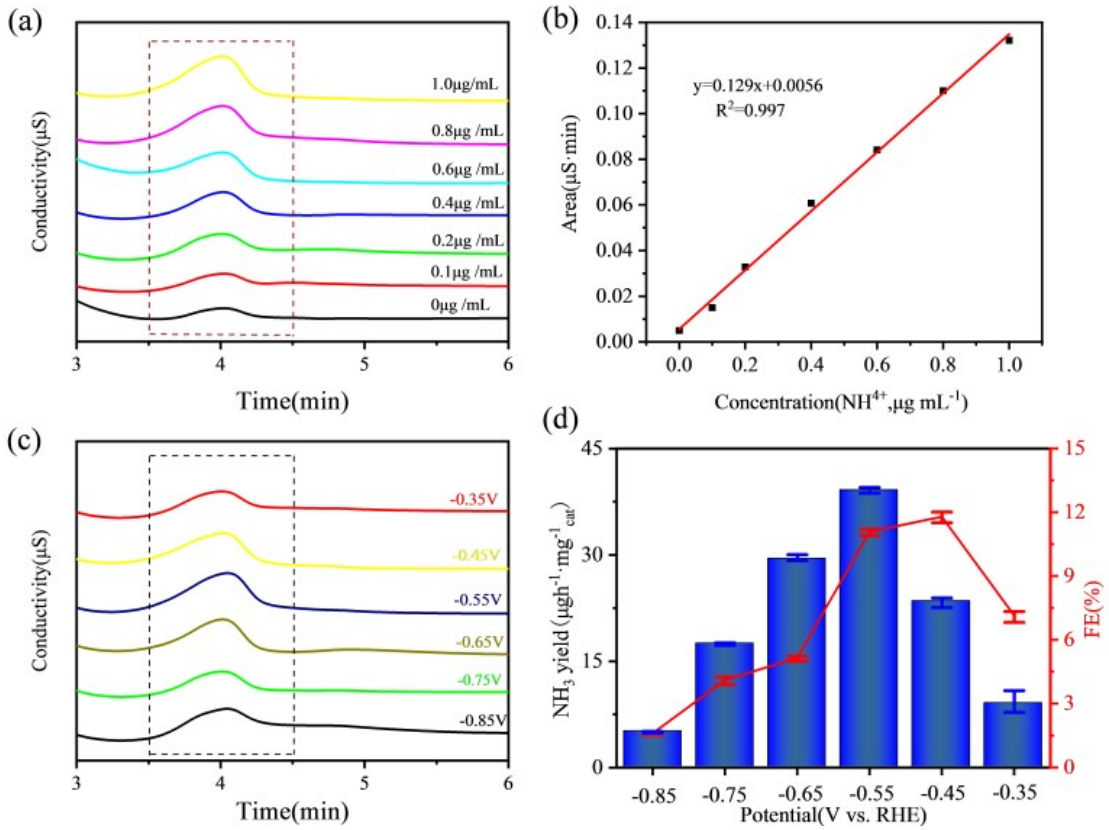

Figure S4. (a) Ion chromatography spectra of NH^{4+} ions with different concentrations. (b) Corresponded calibration curve for NH^{4+}. (c) Ion chromatography of NH^{4+} ions spectra recorded at different potentials. (d) Corresponded FE and NH_3 yield.

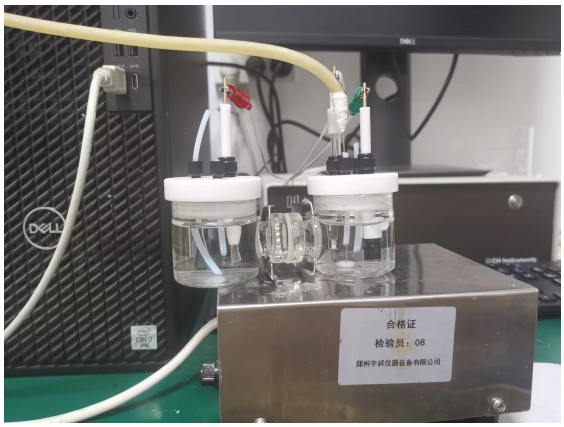

Figure S5. Diagram of electrochemical step for NRR test

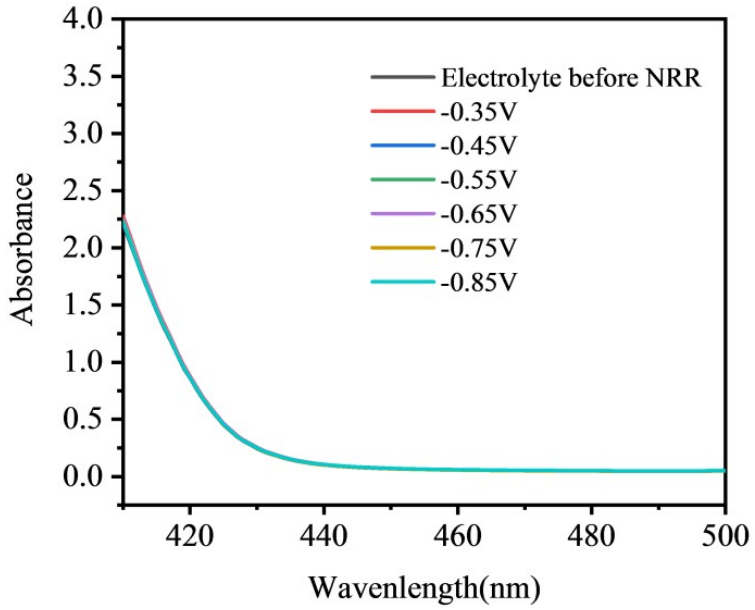

Figure S6. UV-vis absorption spectra of the electrolyte after N_2 electroreduction over Ti_3C_2–B at a series of potentials for 2 h via Watt and Chrisp method.

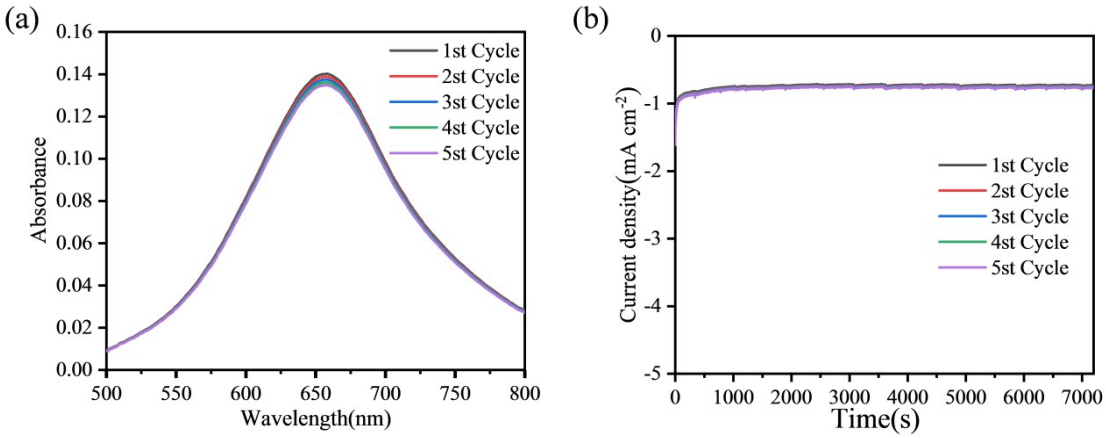

Figure S7. (a) UV-vis absorption spectra of different control experiments stained by indophenol assay for 2 h. (b) NH_3 yields and FEs of Ti_3C_2–B at -0.55 V for five cycles recorded in the N_2-saturated electrolyte.

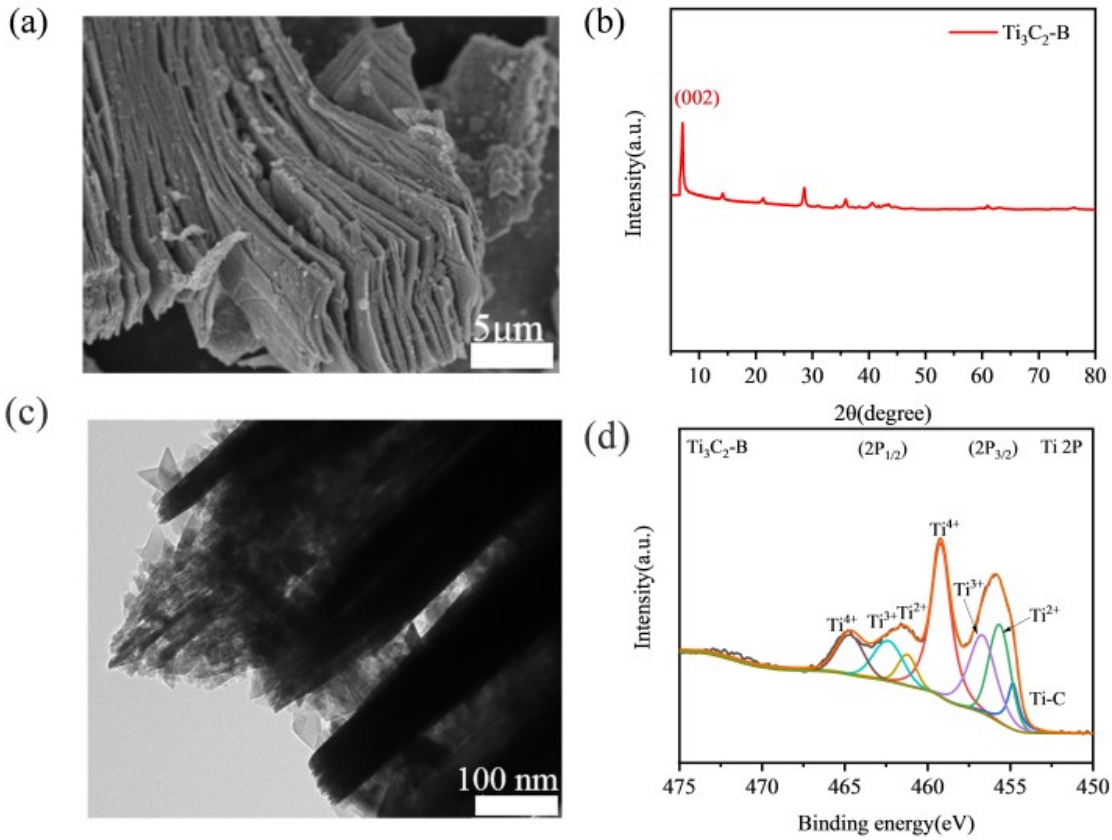

Figure S8. (a) SEM image (b) XRD (c)TEM (d) XPS for Ti_3C_2–B after stability test.

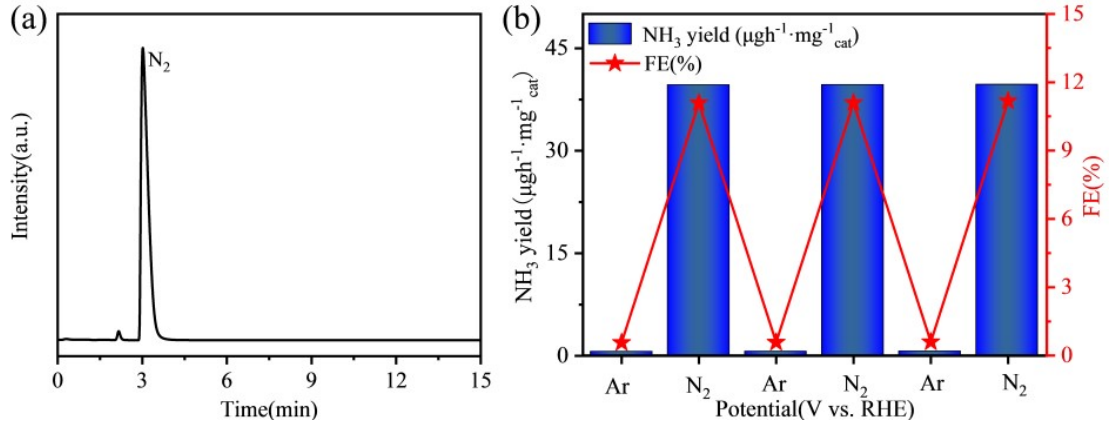

Figure S9. (a) Gas chromatography curves of N_2 (b) NH_3 yields and FEs of Ti_3C_2–B with alternating 2 h cycles between N_2-saturated and Ar-saturated electrolytes at optimum potential (-0.55 V) for a total of 12 h.

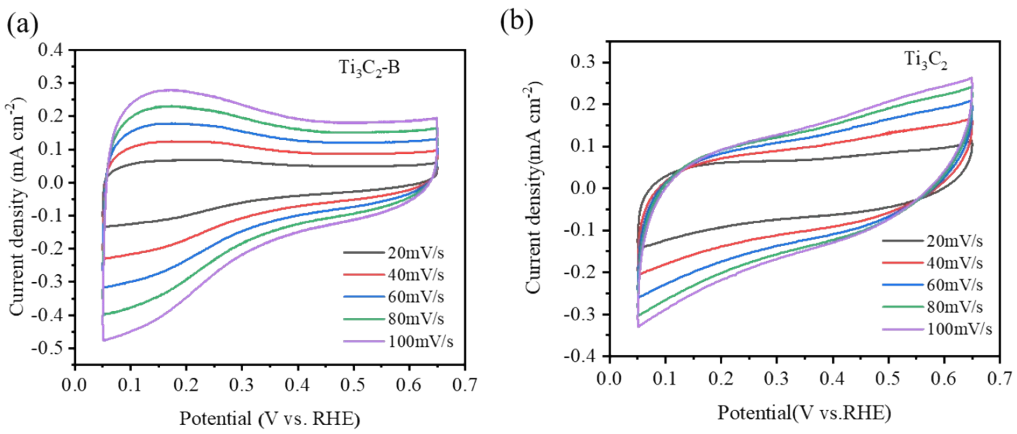

Figure S10. (a) and (b) Cyclic voltammograms (CVs) of Ti_3C_2–B and Ti_3C_2 at different scan rates

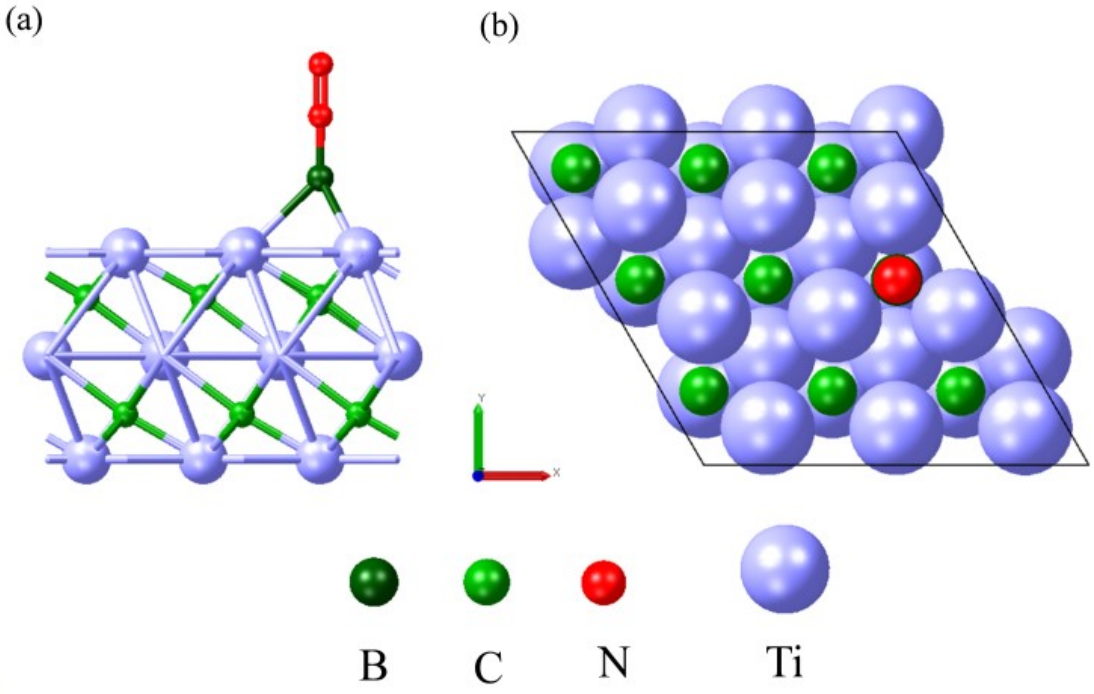

Figure S11. (a) side and (b) top views of Ti_3C_2–B

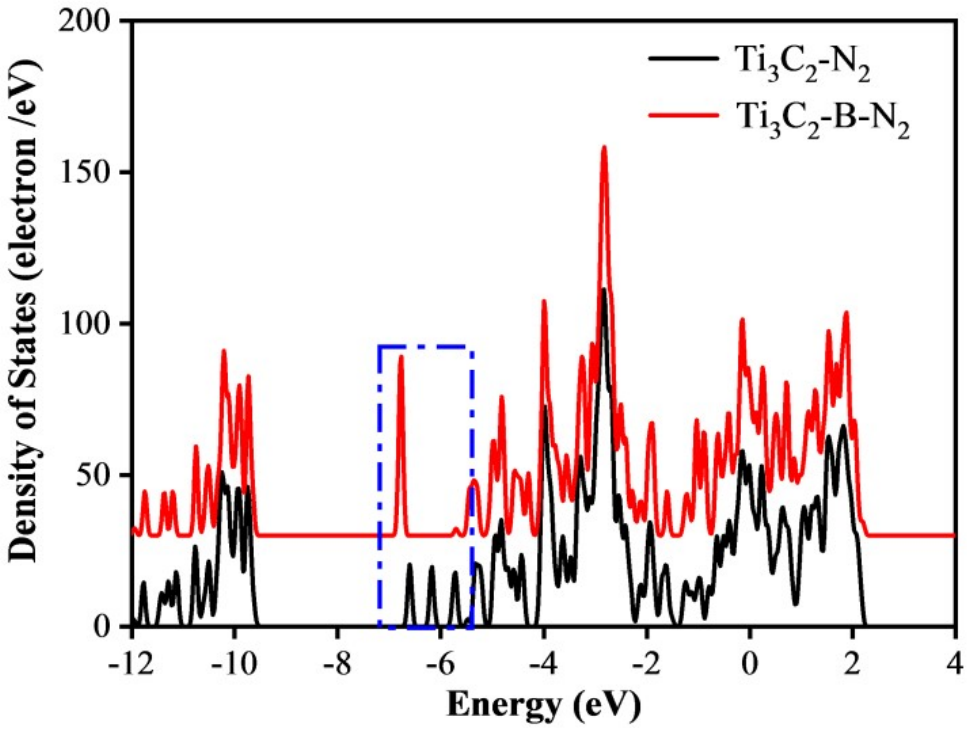

Figure S12. Density of states of the Ti_3C_2–N_2 and Ti_3C_2-B–N_2

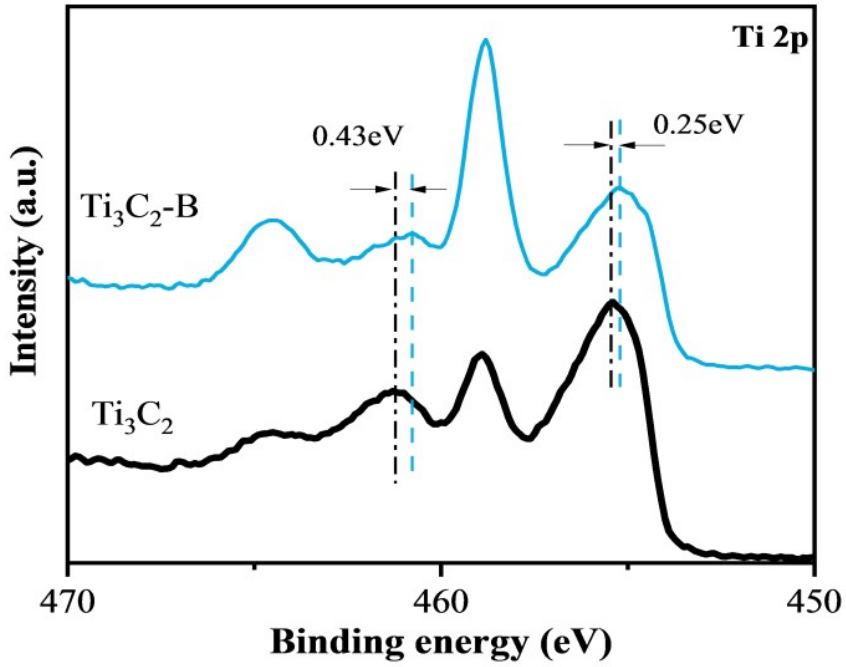

Figure S13. XPS spectra of Ti 2p for Ti_3C_2 and Ti_3C_2-B

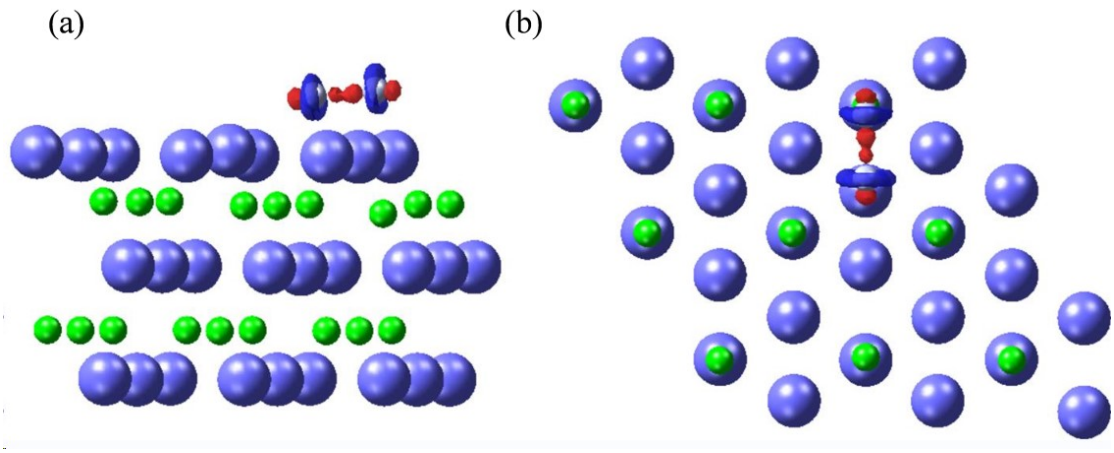

Figure S14. (a) side and (b) top views of charge difference for Ti_3C_2

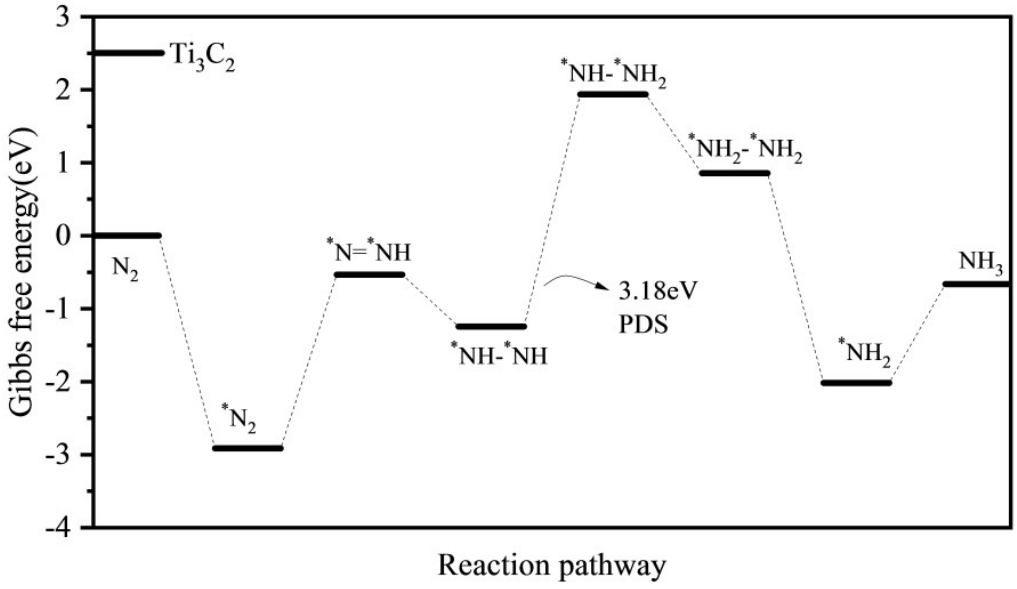

Figure S15. Free energy diagrams of enzymatic NRR pathway on Ti_3C_2

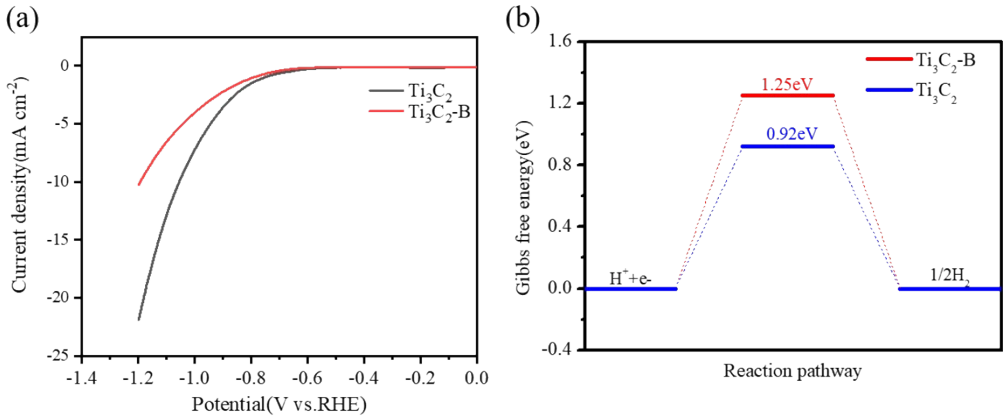

Figure S16. (a) LSV curves of electrocatalytic hydrogen production of $Ti_3C_2$and Ti_3C_2–B. (b) Free-energy scheme of hydrogen evolution reaction on Ti_3C_2 and Ti_3C_2–B respectively.

Table S1. The comparison of Ti_3C_2-B catalyst with the reported catalysts for electrochemical NRR in aqueous solutions.

Catalyst	**Electrolyte**	**NH_3 yield rate ($\mu g h^{-1} mg_{mat}^{-1}$)**	**Faraday Efficiency (%)**	**Ref.**
Ti_3C_2-B	0.05 M H_2SO_4	39.64	11.85	This Work
Mxene-NiCoB	0.1 M Na_2SO_4	38.7	6.92	1
MnO_2-Ti_3C_2	0.1 M HCl	34.12	11.39	2
1T-MoS_2@Ti_3C_2	0.1 M H_2SO_4	30.33	10.94	3
BCN	0.1 M KOH	21.62	9.88	4
Ni-$V_4C_3T_x$	0.1 M KOH	21.29	8.04	5
Au-TiO_{2-x}	0.1M HCl	12.5	10.2	6
Ti_3C_2-medium F	0.01 M Na_2SO_4	3.04	7.4	7

Nb_2O_5/C-800 Mxenes	0.1 M HCl	29.1	11.5	[8]
Pd-TiO_2	0.1 M Na_2SO_4	17.4	12.7	[9]
2.0%Cu/OV-TiO_2	0.05 M H_2SO_4	13.6	17.9	[10]
BiOCl@$Ti_3C_2T_x$	0.1 M HCl	4.06	11.98	[11]
Defective BCN	0.1 M KOH	20.9	18.9	[12]

References

1. C. Wang, Q.-C. Wang, K.-X. Wang, M. De Ras, K. Chu, L.-L. Gu, F. Lai, S.-Y. Qiu, H. Guo, P.-J. Zuo, J. Hofkens and X.-D. Zhu, *Journal of Energy Chemistry*, 2023, **77**, 469-478.
2. W. Kong, F. Gong, Q. Zhou, G. Yu, L. Ji, X. Sun, A. M. Asiri, T. Wang, Y. Luo and Y. Xu, *Journal of Materials Chemistry A*, 2019, **7**, 18823-18827.
3. X. Xu, B. Sun, Z. Liang, H. Cui and J. Tian, *ACS Appl Mater Interfaces*, 2020, **12**, 26060-26067.
4. L. Shi, S. Bi, Y. Qi, G. Ning and J. Ye, *J Colloid Interface Sci*, 2023, **641**, 577-584.
5. C.-F. Du, L. Yang, K. Tang, W. Fang, X. Zhao, Q. Liang, X. Liu, H. Yu, W. Qi and Q. Yan, *Materials Chemistry Frontiers*, 2021, **5**, 2338-2346.
6. P. Yang, H. Guo, H. Wu, F. Zhang, J. Liu, M. Li, Y. Yang, Y. Cao, G. Yang and Y. Zhou, *J Colloid Interface Sci*, 2023, **636**, 184-193.
7. Y. Ding, J. Zhang, A. Guan, Q. Wang, S. Li, A. M. Al-Enizi, L. Qian, L. Zhang and G. Zheng, *Nano Converg*, 2021, **8**, 14.
8. M. Zhang, H. Yin, F. Jin, J. Liu, X. Ji, A. Du, W. Yang and Z. Liu, *Green Energy & Environment*, 2022. **1** 2468-0257.
9. H. J. Chen, G. R. Deng, Z. S. Feng, Z. Q. Xu, M. Y. Yang, Y. Huang, Q. Peng, T. Li and Y. Wang, *Chem Commun (Camb)*, 2022, **58**, 3214-3217.
10. W. P. Utomo, H. Wu and Y. H. Ng, *Small*, 2022, **18**, e2200996.
11. Y. Wang, M. Batmunkh, H. Mao, H. Li, B. Jia, S. Wu, D. Liu, X. Song, Y. Sun and T. Ma, *Chinese Chemical Letters*, 2022, **33**, 394-398.
12. W. Lin, H. Chen, G. Lin, S. Yao, Z. Zhang, J. Qi, M. Jing, W. Song, J. Li, X. Liu, J. Fu and S. Dai, *Angew Chem Int Ed Engl*, 2022, **61**, e202207807.